

Object recognition using three-dimensional optical quasi-correlation

Youzhi Li and Joseph Rosen

Department of Electrical and Computer Engineering, Ben-Gurion University of the Negev, P.O. Box 653, Beer-Sheva 84105, Israel

Received January 30, 2002; revised manuscript received April 16, 2002; accepted April 24, 2002

A novel method of three-dimensional (3-D) object recognition is proposed. Several projections of a 3-D target are recorded under white-light illumination and fused into a single complex two-dimensional function. After proper filtering, the resulting function is coded into a computer-generated hologram. When this hologram is coherently illuminated, a correlation space is reconstructed such that light peaks indicate the existence and locations of true targets in the observed 3-D scene. Experimental results and comparisons with results of another 3-D object recognition technique are presented. © 2002 Optical Society of America

OCIS codes: 100.6890, 100.5090, 100.5010, 100.4550, 110.6880, 110.4190, 090.1760, 090.2870.

1. INTRODUCTION

Since the pioneer work of VanderLugt¹ almost 40 years ago, optical two-dimensional (2-D) correlation techniques have been proved to be useful in various image-processing applications, such as pattern recognition and target tracking. Recently there has been increasing interest in three-dimensional (3-D) optical information processing because of its potential applications. A method for performing 3-D optical correlation was first proposed by Bamler and Hofer-Alfeis.² In their study, the 3-D observed scene is first mapped, slice by slice along its longitudinal axis, onto a large 2-D plane. Then conventional 2-D optical correlations are performed between every slice and all the others. In this method the observed scene must be processed with intensive digital algorithms to reconstruct the 3-D image inside the computer memory before any correlation can be employed.

Recently, other attempts at 3-D optical pattern recognition have been reported.^{3-8,10,11} Rosen has proposed to extend the correlation dimensions from 2-D to 3-D by introducing 3-D optical Fourier transform^{3,4} (FT). By fusion of several projections of the tested scene, a 3-D object function is first Fourier transformed, then filtered by some 3-D reference filter, and finally inversely Fourier transformed into the correlation space. By this technique a target can be detected and located in its 3-D environment. Rosen's method was first demonstrated with a 3-D joint transform correlator⁵ (JTC). Later, the present authors proposed a method to implement 3-D distortion invariance for the 3-D pattern recognition by use of a single 2-D synthetic reference function in the 3-D JTC.⁶ As an alternative to the 3-D JTC, we also proposed a hybrid 3-D correlator with general complex filters.⁷ Esteve-Taboada *et al.* introduced into the 3-D object recognition⁸ the Fourier transform profilometry technique.⁹ A grating pattern is projected onto a 3-D object surface, and a digital camera captures the observed 2-D image of the scene. The obtained deformed grating patterns contain the information on the 3-D object's struc-

ture. These captured patterns are correlated with reference functions by a conventional 2-D optical correlator so that the targets can be recognized at the observed scene. Frauel *et al.* proposed a different 3-D object recognition technique using digital holography.¹⁰ First various 2-D viewpoint projections of the 3-D observed scene are reconstructed from a digital hologram. Then the system recognizes the true targets included in the tested 3-D scene by use of 2-D correlation techniques. Matoba *et al.* captured multiple perspectives of 3-D objects by a microlens array.¹¹ The various perspectives of the reference and the input scene are cross correlated by a 2-D JTC, whereas the depth information of the 3-D objects is converted to angular information on the perspectives.

The main criticism of all the various versions of the 3-D correlators developed at Ben-Gurion University³⁻⁷ (in the following we term them all BGU correlators) has been directed against their complexity and their extensive use of digital computation. To overcome these drawbacks, we propose here a new 3-D pattern recognition system, termed 3-D optical quasi-correlator (OQC). This system is a degenerate version of the hybrid BGU correlator.⁷ It can still recognize and locate objects in 3-D space, and thus the 3-D space invariance property is maintained. However, the recognition in the 3-D OQC is not done by a complete 3-D correlation. Therefore in a few respects, such as simplicity and operation speed, the new system is superior to the BGU correlators. However, there is some penalty for this simplicity in reduction of the system's performance. For instance, the signal-to-noise ratio (SNR) is reduced compared with its value in the BGU correlators, as will be demonstrated in Section 3.

The main difference between the 3-D OQC and the BGU correlators exists in their output. In the BGU correlators each transverse slice of the 3-D correlation space is reconstructed separately from a different computer-generated hologram (CGH). In the 3-D OQC, on the other hand, only a single CGH is used to reconstruct the intensity distribution of the entire 3-D correlation space at once. Therefore the method of detecting the correla-

tion peaks should be modified. The correlation peaks are not necessarily distributed on a single transverse plane that can be recorded by a conventional planar detector. Instead, one needs an imaging system that is capable of observing the entire 3-D correlation space. Such a system can be, for instance, the human vision system, which enables anyone with stereoscopic vision to observe the correlation peaks and estimate their locations in the 3-D space. An artificial imaging system, which imitates this kind of human ability, is an additional option that should be considered in this context.

2. ANALYSIS OF THE SYSTEM

The image-capturing processes by the 3-D OQC and by the BGU correlators are identical, and such a process has already been described in Ref. 7. Nevertheless, for completeness, we repeat the description of this part in the following.

The complete proposed scheme is shown in Fig. 1. The input function containing several objects is denoted by $o_1(x, y, z)$, where (x, y, z) are the coordinates of the observed scene. A digital camera, located a distance L from the origin, captures the objects $o_1(x, y, z)$ from several different points of view. The digital camera is shifted in constant angular steps along a horizontal arc centered on the origin, where the camera is always directed to the origin. The angle between the optical axis of the digital camera and the z axis is denoted by θ_i . For each θ_i , the projected image $o_2(x_i, y_i, \theta_i)$ is recorded into the computer, where (x_i, y_i) are the coordinates of the image plane of each camera. Based on simple geometrical considerations, the relation between (x_i, y_i) and (x, y, z, θ_i) is given by

$$(x_i, y_i) = M(x \cos \theta_i + z \sin \theta_i, y), \tag{1}$$

where M is the magnification factor of the digital camera. Assuming that the distance L is much longer than the depth of the 3-D input scene, all the object points of the 3-D input scene are equally imaged with the same magnification factor M .

Inside the computer, the processing is different from that of the BGU correlators. In the BGU correlators the computation process of the angular projections has yielded a 3-D FT of the scene. Then, after appropriate filtering and another 3-D FT, we obtained 3-D correlation between a reference and the scene objects. Here the output stage of the OQC is different from that of the BGU correlators, and therefore the computational processing is changed. In the OQC output, a Fourier hologram is coherently illuminated, and as a result, the 3-D correlation space is reconstructed in front of the observer's eyes. The desired hologram has only two dimensions, even though it represents a 3-D scene, and therefore the 3-D data of the angular projections should be compressed properly into a two-dimensional function. This compression is the goal of the computational process, as described next.

The set of captured images are compressed in a special way to a single spectral matrix. The digital operations along the horizontal and the vertical axes are different because the camera collects the angular projections only along the horizontal axis. As the following analysis shows, the entire spatial spectrum information from every projection along the x_i axis is redundant. For each k th projection from the view angle θ_k we just calculate, and store, the spectral content of the u_k th frequency element, where $u_k = \theta_k/a$ and a is some chosen parameter. In other words, from the spatial spectrum of each projected image a different column is picked up according to the above-mentioned rule. Of course, there is no need to calculate the complete horizontal spectrum of every projection, but only the columns from the spectrum that are used in the new obtained matrix. Each k th projection is multiplied by $\exp(-j2\pi x_i u_k / \lambda f)$, and the product is summed along the rows (i.e., along x_i) to a single column. λ is the wavelength of a plane wave illuminating the output hologram, and f is the focal length of the spherical Fourier lens used later in the system's output. As we show below, the parameter a controls the longitudinal magnification of the correlation space independently of the transverse magnification. In this stage, the entire projected matrices are compressed to a single 2-D matrix, which is then Fourier transformed along the y_i axis, with a scale factor of $1/(\lambda f)$. Thus, in continuous formalism, the dimensions of the grabbed data are reduced from three to two in the following way:

$$o_3(u, v) \propto \iint o_2(x_i, y_i, au) \exp[-j2\pi \times (ux_i + vy_i)/\lambda f] dx_i dy_i. \tag{2}$$

Note that there is no Fourier transform along x_i , because for each frequency value u the integration is done on a different projection according to the relation $\theta_i = au$. The complete computational process is illustrated schematically in Fig. 2. It should be noted that although the rule

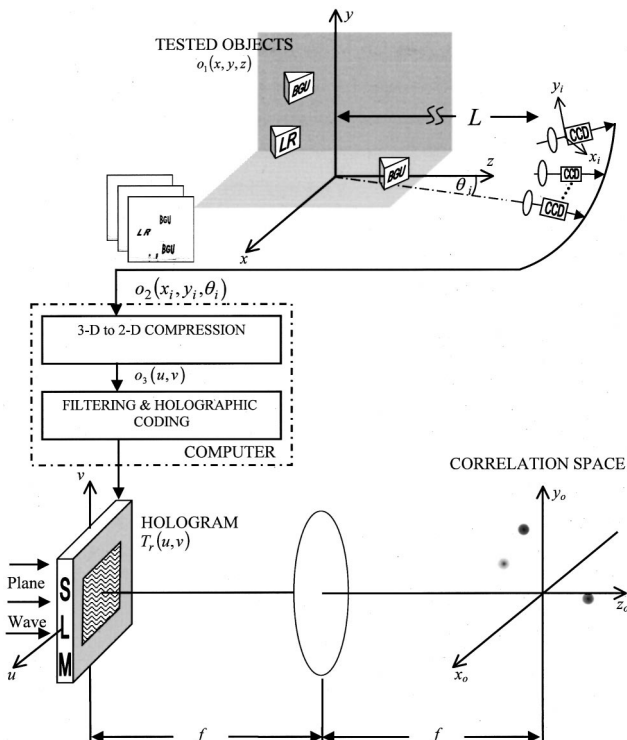


Fig. 1. Schematic of the proposed system.

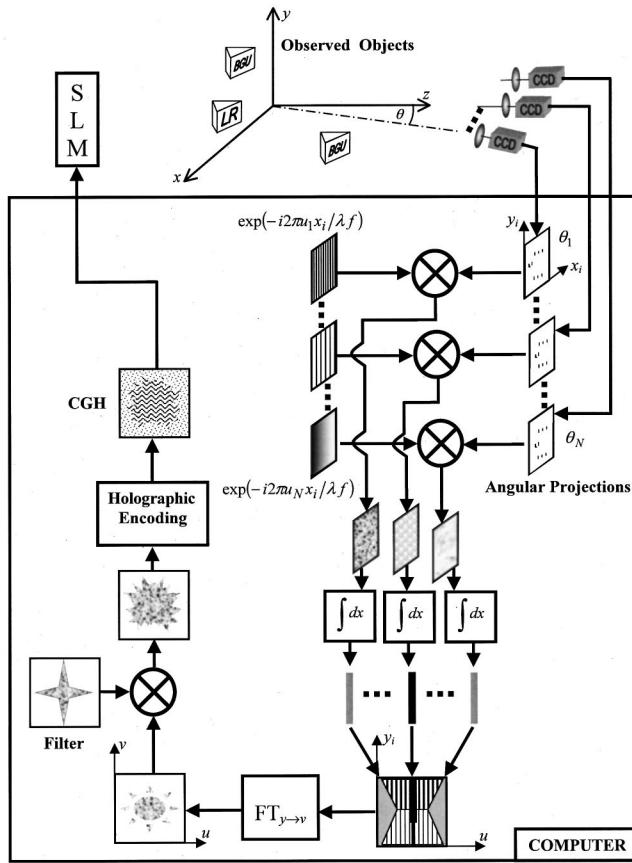


Fig. 2. Schematic of the computational process from capturing the projections to displaying the hologram.

for compressing seems arbitrary, the relation $\theta_i = au$ leads to the desired Fourier hologram, as shown in the following.

The maximum view angle θ is chosen to be small (in the current example, it is 16° from each side of the z axis), and thus we can employ the small-angle approximation: $\cos \theta_i \approx 1$ and $\sin \theta_i \approx \theta_i$. Substituting Eq. (1), the small-angle approximations, and the relation $\theta_i = au$ into relation (2) yields

$$o_3(u, v) \propto \int \int o_2(x_i, y_i, au) \exp[-j2\pi M \times (ux + vy + au^2z)/\lambda f] dx_i dy_i. \quad (3)$$

Let us look at a single element from the entire 3-D object function. This infinitesimal element of the size $(\Delta x, \Delta y, \Delta z)$ at point (x, y, z) and with brightness $o_1(x, y, z)$ appears as a single element on every projection plane, but at a different location from projection to projection according to Eq. (1). Therefore in this case the spectrum presented in relation (3) is given by

$$o_3(u, v) \propto o_1(x, y, z) \exp[-j2\pi M \times (ux + vy + au^2z)/\lambda f] \Delta x \Delta y \Delta z. \quad (4)$$

Next we examine the influence of all points of the tested scene $o_1(x, y, z)$ on the distribution of $o_3(u, v)$. The tested scene is three-dimensional, and therefore the overall distribution of $o_3(u, v)$ is obtained as a 3-D integral of all the points from the input scene, as follows:

$$o_3(u, v) \propto \int \int \int o_1(x, y, z) \exp[-j2\pi M \times (ux + vy + au^2z)/\lambda f] dx dy dz. \quad (5)$$

Thus we obtain a 2-D function, which contains 3-D information from the tested scene similarly to the way that a 2-D optical hologram contains the 3-D information of the recorded 3-D scene.¹² First $o_3(u, v)$ is multiplied by a proper filter, and then the obtained product is encoded into a CGH. The CGH, when illuminated by a plane wave, yields a holographic reconstruction of the correlation space, as shown in the lower part of Fig. 1. Thus we can detect the targets and also locate them in their 3-D environment.

To implement the 3-D object recognition we consider next the filter function defined by

$$F(u, v) \propto \int \int \int f^*(-x, -y, -z) \exp[-j2\pi M \times (ux + vy + au^2z)/\lambda f] dx dy dz, \quad (6)$$

where $f(x, y, z)$ is the spatial reference function located at the origin of the coordinate system (x, y, z) and the asterisk denotes complex conjugate. Multiplying $o_3(u, v)$ given by relation (5) with the filter function given by relation (6) yields

$$\begin{aligned} T(u, v) &= o_3(u, v) F(u, v) \\ &\propto \int \int \int o_1(x, y, z) \exp[-j2\pi M \times (ux + vy + au^2z)/\lambda f] dx dy dz \\ &\quad \times \int \int \int f^*(-\xi, -\eta, -\zeta) \exp[-j2\pi M \times (u\xi + v\eta + au^2\zeta)/\lambda f] d\xi d\eta d\zeta \\ &= \int \int \int \int \int o_1(x, y, z) f^*(-\xi, -\eta, -\zeta) \\ &\quad \times \exp[-j2\pi M \{u(x + \xi) + v(y + \eta) + au^2(z + \zeta)/\lambda f\}] dx dy dz d\xi d\eta d\zeta \\ &= \int \int \int \int \int o_1(x, y, z) f^*(x - \hat{x}, y - \hat{y}, z - \hat{z}) dx dy dz \\ &\quad \times \exp[-j2\pi M (u\hat{x} + v\hat{y} + au^2\hat{z})/\lambda f] d\hat{x} d\hat{y} d\hat{z} \\ &= \int \int \int g(\hat{x}, \hat{y}, \hat{z}) \exp[-j2\pi M (u\hat{x} + v\hat{y} + au^2\hat{z})/\lambda f] d\hat{x} d\hat{y} d\hat{z}, \end{aligned} \quad (7)$$

where

$$\begin{aligned} g(\hat{x}, \hat{y}, \hat{z}) &= \int \int \int o_1(x, y, z) f^*(x - \hat{x}, y - \hat{y}, z - \hat{z}) dx dy dz, \\ \hat{x} &= x + \xi, \quad \hat{y} = y + \eta, \quad \hat{z} = z + \zeta. \end{aligned} \quad (8)$$

The function $g(\hat{x}, \hat{y}, \hat{z})$ is the 3-D correlation between the tested object function and the reference function. The 2-D function $T(u, v)$ is generally complex valued, and in this stage it is stored inside the computer memory.

Looking over the last line of relation (7) we note that there is no symmetry between the horizontal coordinate u and the vertical coordinate v . In the argument of the exponent, one finds the term au^2z without the term av^2z . This is because the recording process is not symmetric since all the recorded projections are horizontal-only viewpoints. If we could collect all the projections along the horizontal as well as the vertical viewpoints, relation (7) would become symmetrical. In such a hypothetical case the function $T(u, v)$ could become

$$\begin{aligned} \tilde{T}(u, v) = & \int \int \int g(\hat{x}, \hat{y}, \hat{z}) \exp\{-j2\pi M \\ & \times [u\hat{x} + v\hat{y} + a(u^2 + v^2)\hat{z}]/\lambda f\} d\hat{x}d\hat{y}d\hat{z}. \end{aligned} \tag{9}$$

In order to understand the way that the correlation function $g(\hat{x}, \hat{y}, \hat{z})$ can be obtained from $\tilde{T}(u, v)$, we have to look for an equivalent optical system that yields the same distribution of $\tilde{T}(u, v)$. Such system is well known in the literature for the parameter value $a = -1/2f$. When $g(\hat{x}, \hat{y}, \hat{z})$ is located in the vicinity of the front focal point of a spherical lens and illuminated by a plane wave, the 2-D complex amplitude on the back focal plane of this lens is equal to $\tilde{T}(u, v)$ given by Eq. (9) (Ref. 13) for $a = -1/2f$. Therefore, on the basis of the principle of optical reciprocity, if $\tilde{T}(u, v)$ located at the front focal plane is encoded as a hologram and this hologram is illuminated by a plane wave, the 3-D distribution $g(\hat{x}, \hat{y}, \hat{z})$ is reconstructed in the vicinity of the back focal point of the lens. $g(\hat{x}, \hat{y}, \hat{z})$, as mentioned above, is the 3-D spatial distribution of the cross correlation between the object function $o_1(\hat{x}, \hat{y}, \hat{z})$ and the reference function $f(\hat{x}, \hat{y}, \hat{z})$. Note that choosing a different value for the parameter a changes only the proportions between the transverse and the longitudinal dimensions of the reconstructed space, as already discussed in Ref. 12.

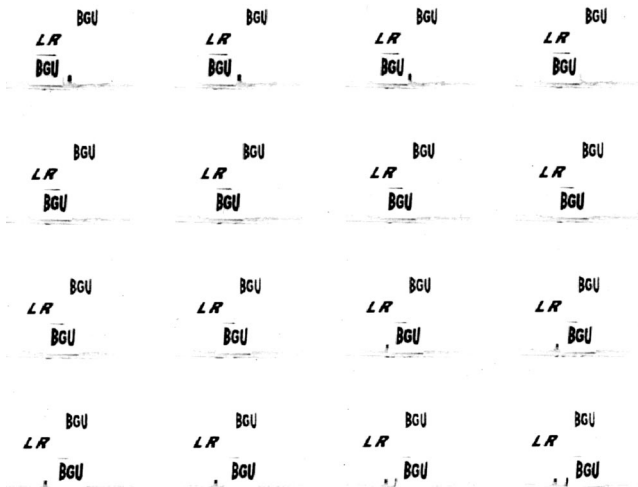
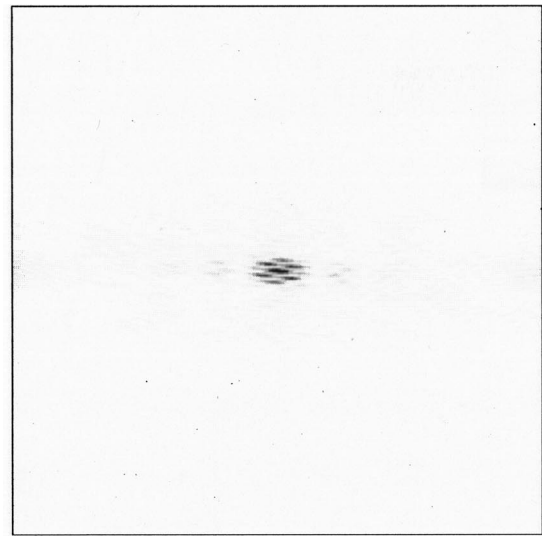
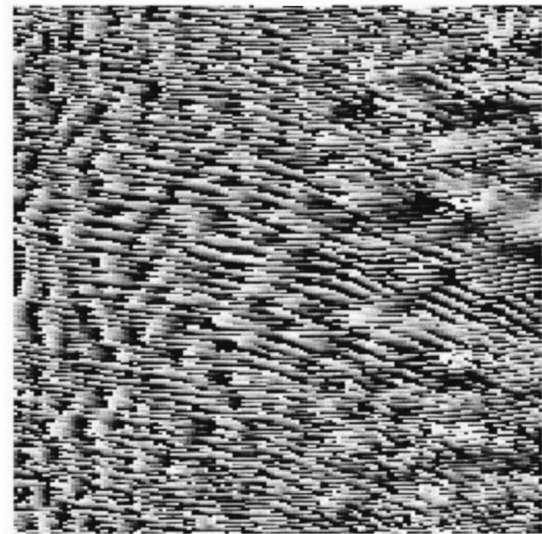


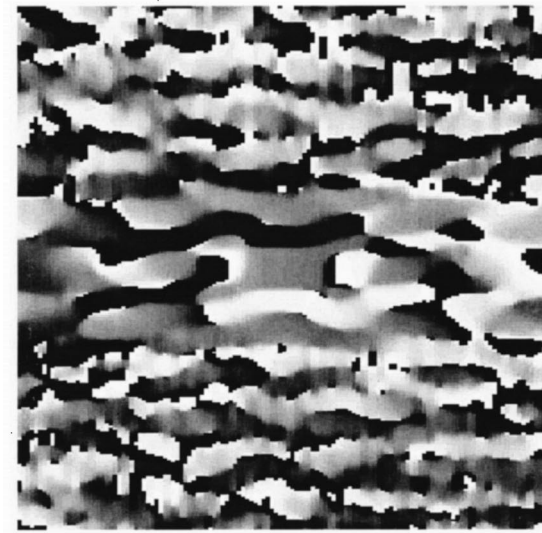
Fig. 3. Sixteen out of sixty-five projections of the tested scene, imaged from -16° to 16° .



(a)



(b)



(c)

Fig. 4. (a) Amplitude and (b) phase function of the compressed spatial spectrum of the scene; (c) phase function of the 3-D POF.

Unfortunately because of the scanning direction along the horizontal axis only, the distribution that we can encode into a hologram is $T(u, v)$ but not $\tilde{T}(u, v)$. As a result, the system inherently suffers from astigmatism: the correlation peaks are focused in different locations along the x and y axes. Because of the term of au^2z the peaks are focused along the horizontal axis in the locations of the true objects at the input space, whereas because of missing of the term of av^2z the same correlation peaks are focused along the vertical axis on the back focal plane of the reconstructing lens. This means that if a true object is located somewhere out of the origin, its correlation peak appears out of the back focal plane as a small line along the vertical axis instead of a point. The location of an object along the longitudinal axis should be identified according to the measure of focusing along the horizontal axis only.

The astigmatism described above is one reason for the lower SNR in comparison with that of the BGU correlator. As mentioned above, the astigmatism is avoidable if the scanning of the input scene is performed along all the directions of a transverse plane. Therefore the astigmatism can be considered a preventable problem that can be removed with an improved technology. However, there is an unavoidable source of noise that is inherent in the holographic reconstruction. When there are several true objects distributed in the scene in different transverse planes, the beam, which creates a correlation peak for each true object, passes through all the rest of transverse planes and induces noise on all of them. This phenomenon distinguishes the obtained QOC holographic reconstruction from the real 3-D cross-correlation distribution obtained by the BGU correlators, and this is the reason that the QOC is considered a quasi-correlator only.

As mentioned above, the hologram values are memorized inside the computer in a form of the complex function $T(u, v)$. For reconstruction of the correlation space

from the complex function, the computer should modulate some transparency medium with $T(u, v)$ values. In case the transparency cannot be modulated directly with complex values, one of many well-known coding methods of CGH's¹⁴ might be used. The spatial light modulator (SLM) that we use in this study can modulate an incident wave with positive gray tones. Therefore the complex function $T(u, v)$ is coded into a positive real transparency as follows,

$$T_r(u, v) = 0.5 \left(1 + \operatorname{Re} \left\{ T(u, v) \exp \left[\frac{j2\pi}{\lambda f} (d_x u + d_y v) \right] \right\} \right), \quad (10)$$

where (d_x, d_y) is the new origin point of the reconstruction space and $|T(u, v)|$ is normalized between 0 and 1.

The holographic reconstruction setup is shown in the lower part of Fig. 1. The SLM modulated by $T_r(u, v)$ is illuminated by a plane wave, which propagates through the Fourier lens toward the observer. $T_r(u, v)$ given in Eq. (10) contains, among others, the term $T^*(u, v)$. From a Fourier transform of this term one can get the output correlation peaks with the same orientation as the original objects in the vicinity of the point $(x_0, y_0, z_0) = (-d_x, -d_y, 0)$, where $z_0 = 0$ designates the back focal plane of the Fourier lens.

3. EXPERIMENTAL RESULTS

To test our proposed scheme, we carried out an experiment, as described next. In this preliminary experiment, the tested 3-D scene included three objects with labels on their front faces, shown in the upper part of the Fig. 1. Two of them with the letters BGU on their faces were the true targets that should be detected by the proposed sys-

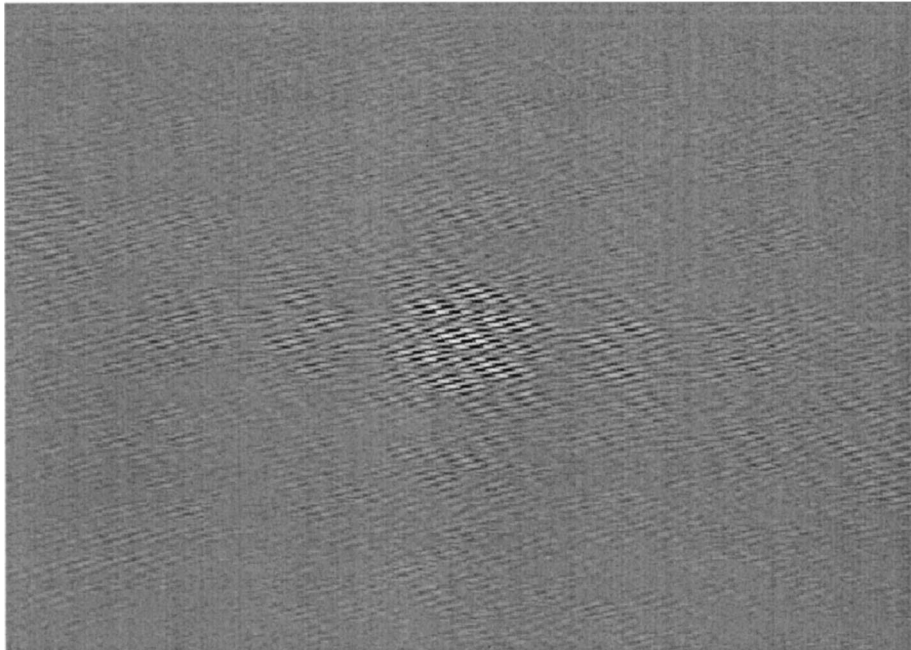


Fig. 5. Central part of the CGH generated from $T(u, v)$ by use of the holographic coding method.

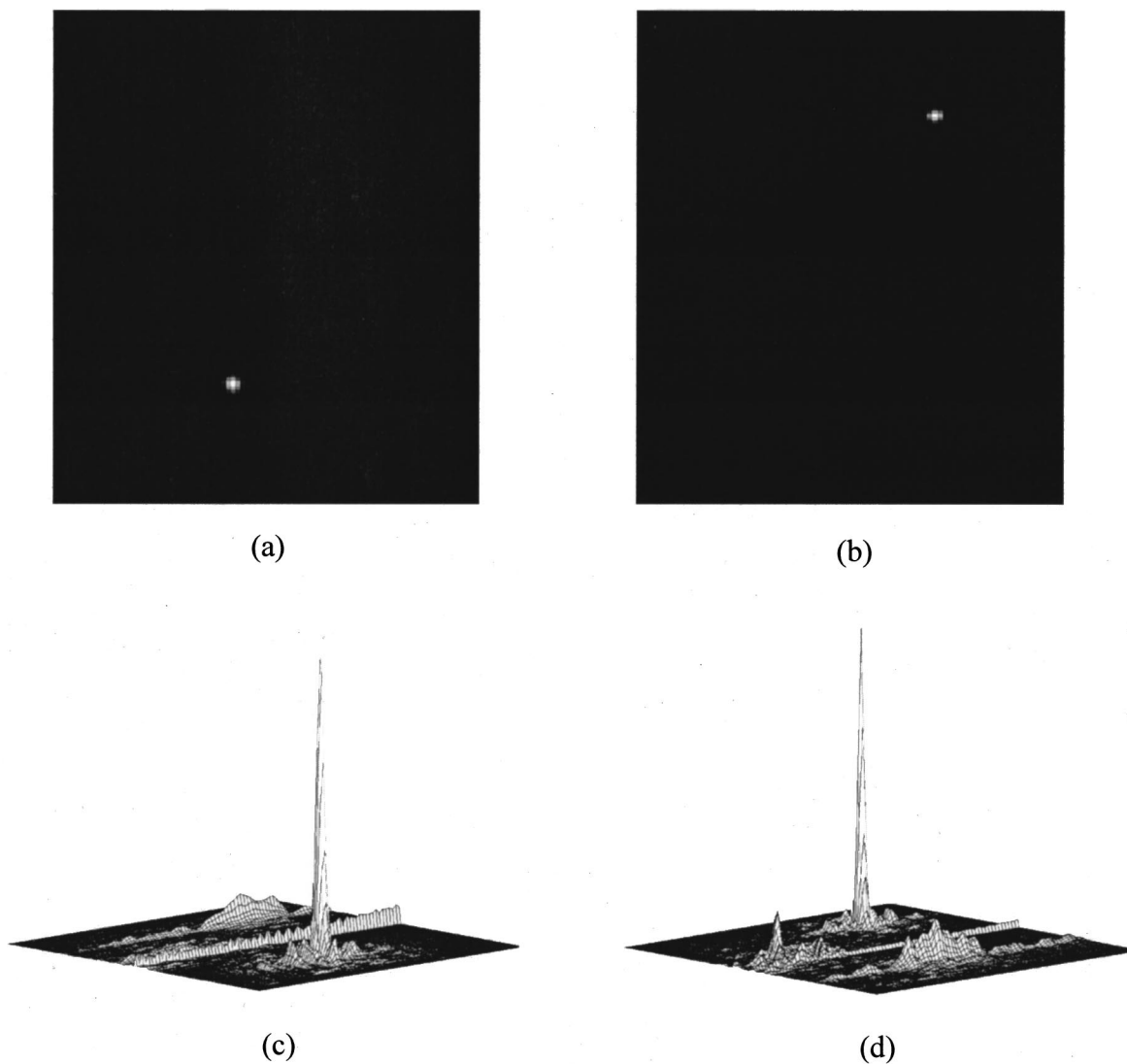


Fig. 6. Simulated correlation results recorded at (a) $z = 12.5$ pixels, (b) $z = -12$ pixels; (c) and (d) are the 3-D plots of (a) and (b), respectively.

tem. The lower front object was located at the point $(x, y, z) = (0, 0, 5.6)$ cm, whereas the higher back object was put at the point $(-3, 12.5, -5.4)$ cm (both with the letters BGU). The object with the letters LR located at the point $(3, 8.5, -5.4)$ cm was used as the false target. This object should be ignored by the system. One digital camera observed the scene from a distance $L = 120$ cm from the origin of the tested scene. The camera was shifted along an arc centered at the origin. At each position, the camera was always directed toward the origin and captured each projected image into a computer. The total view angle interval was 32° , 16° for each side of the z axis. The camera was shifted by 0.5° from point to point. Thus, 65 projections of the 3-D tested scene were recorded into the computer; 16 of them are depicted in Fig. 3 with a gap of 2° between every two consecutive projections. The spectral matrix $o_3(u, v)$ generated from these data is shown in Fig. 4, where Figs. 4(a) and 4(b) are its amplitude and phase angle, respectively.

The reference object was located at the origin of the scene and was imaged into the computer by the method

described above; i.e., the observed reference object was recorded 65 times from different viewpoints by the CCD into the computer. From the recorded projections of the reference object we calculated a phase-only filter (POF), first by calculating the spectral matrix according to relation (2) and then by taking only the phase distribution of this matrix. The phase distribution of the POF function $F(u, v)$ is shown in Fig. 4(c). The multiplication result $T(u, v)$, of $o_3(u, v)$ by $F(u, v)$, was then encoded as a CGH $T_r(u, v)$ according to Eq. (10). The central part of the obtained hologram is shown in Fig. 5. To reconstruct the correlation space, we carried out both simulation and optical experiment. Figure 6 shows the correlation results of the simulation, and the peaks in Figs. 6(a) and 6(b) indicate the existence and locations of the front and the back true targets. Figures 6(c) and 6(d) are the 3-D plots of the intensity distributions on the two planes shown in Figs. 6(a) and 6(b), respectively. The false target never generated a meaningful peak. In the optical experiment, the obtained CGH was displayed on the SLM and was illuminated by a plane wave as shown in the

lower part of Fig. 1; the correlation results were reconstructed from the CGH and are depicted in Fig. 7. Figure 7(a) recorded at $z_0 = 2.6$ cm shows the correlation peak of the front true target, and Fig. 7(b) recorded at $z_0 = -2.5$ cm depicts the correlation peak of the back true target. The false target still never generated a meaningful correlation peak. The 3-D plots of Figs. 7(a) and 7(b) are depicted in Figs. 7(c) and 7(d), respectively. The experimental results are consistent with the simulation results, although the optical reconstruction system induces noise, which is not predicted by the simulation.

From the obtained correlation results one can easily detect the two true targets, and locate them as well, in their 3-D space. The correlation strength along z_0 axis is also investigated in this experiment. The intensities of the correlation peaks along z_0 axis, at their maximal transverse points, are shown in Fig. 8.

The proposed system was compared with the results of the hybrid BGU correlator⁷ with two kinds of filters and with two measures. One measure of the performance is SNR indicating the discrimination capability and defined by

$$\text{SNR} = \frac{\text{maximum correlation peak intensity of the true target}}{\text{maximum noise intensity}}. \quad (11)$$

Another criterion is peak-to-correlation energy¹⁵ (PCE) indicating the correlation peak sharpness and defined by

$$\text{PCE} = \frac{\text{maximum correlation peak intensity of the true target}}{\text{average correlation plane energy}}, \quad (12)$$

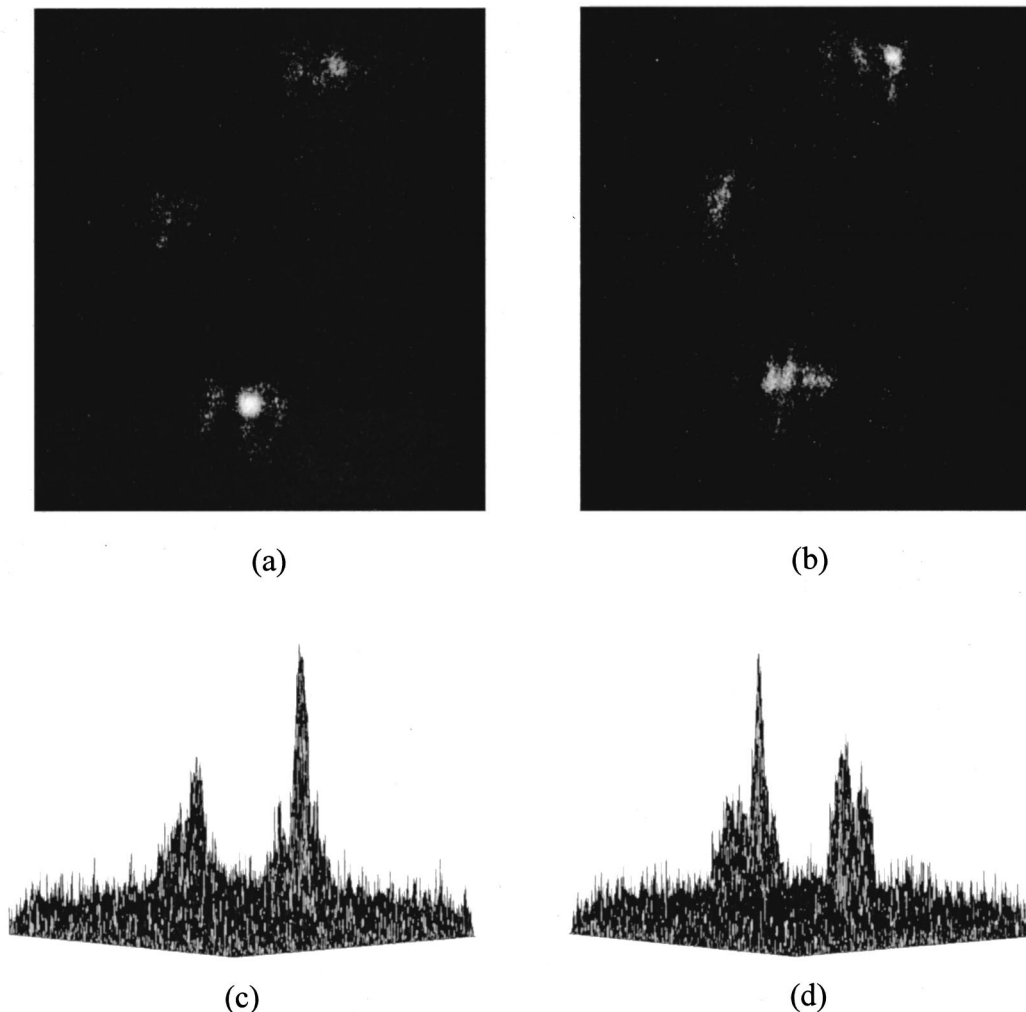


Fig. 7. Experimental correlation results recorded at (a) 2.6 cm and (b) -2.5 cm along the z axis; their 3-D plots are shown in (c) and (d), respectively.

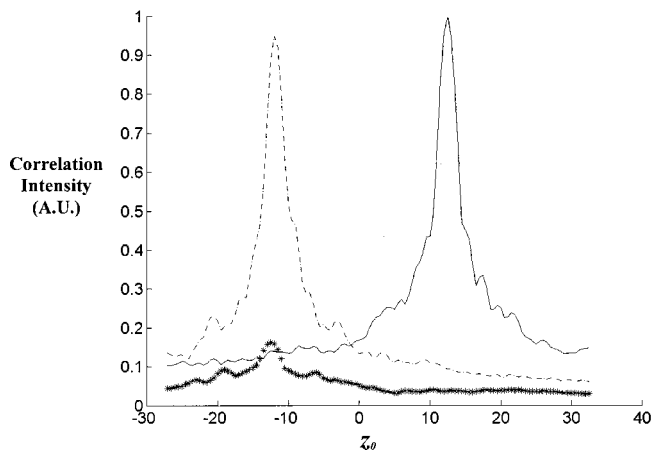


Fig. 8. Simulated correlation plots along the z_0 axis. Dotted-dashed curve, case of the back true object, the asterisk curve, false object; and solid curve, front true object.

Table 1. Summary of SNR and PCE between the Hybrid BGU Correlator and the 3-D OQC for Two Kinds of Filters

Performance Criteria	Filters	3-D OQC	BGU Correlator
SNR	Matched Filter	1.8	17.8
	POF	7.3	21.6
PCE	Matched Filter	179.6	1493.6
	POF	1499.7	3647.1

where the average correlation plane energy is defined as the sum of the entire correlation plane intensity divided by the total number of pixels on a correlation plane. The two criteria are defined on some specific transverse planes where the peaks of the true objects are maximal. We employed different filters such as the conventional matched filter and the POF in both 3-D OQC and the hybrid BGU correlator in order to compare their performances. The SNR and the PCE are calculated accordingly and are summarized in Table 1. The SNR and the PCE for 3-D OQC are summarized in column 3 and those for BGU correlators in column 4. From Table 1, one can conclude that although the performances of 3-D OQC are acceptable for different filters, the performances of BGU correlators are superior. This is a reasonable penalty, owing to the use of less information in 3-D OQC than that in the BGU correlators. However, as mentioned above, when the imaging process is carried out along the entire transverse directions, the generated hologram will be $\tilde{T}(u, v)$ rather than $T(u, v)$. Thus the above-mentioned astigmatism will be eliminated and the performances of 3-D OQC can be improved.

4. CONCLUSION

In conclusion, we have proposed a novel method named 3-D OQC to implement 3-D object recognition. By fusion of several projections of the tested scene and with proper filtering, a 2-D hologram of the correlation between the tested scene and the reference function is digitally generated. The correlation results are reconstructed when the single hologram is coherently illuminated. The simplic-

ity and speed of the OQC are superior to those of the BGU correlators. However, because less information is used in the 3-D OQC than in the BGU correlators, the method suffers from some penalty of lower SNR and lower PCE in comparison with the BGU correlators. The OQC performances can be improved when a symmetrical scanning process is carried out. The method of a single hologram is general and is applicable even in circumstances where the objects are occluded from some viewpoints or their shapes are changed as the camera moves. This generality statement is based on our knowledge about holograms of 3-D objects, which can image partially occluded objects from certain points of view.

Another unique motivator in this study is the nature of the 3-D correlation space. To the best of our knowledge, this is the first time that anyone has suggested and demonstrated a reconstruction of 3-D correlation space from a single hologram. This innovation should be accompanied by a new concept of detection of the correlation results. One possible option is to let a human observer look over the correlation space and estimate the locations of all the true targets in the scene.

Corresponding author Joseph Rosen can be reached by e-mail at rosen@ee.bgu.ac.il.

REFERENCES

1. A. Vanderlugt, "Signal detection by complex spatial filtering," *IEEE Trans. Inf. Theory* **IT-10**, 139–145 (1964).
2. R. Bamler and J. Hofer-Alfeis, "Three- and four-dimensional filter operations by coherent optics," *Opt. Acta* **29**, 747–757 (1982).
3. J. Rosen, "Three-dimensional optical Fourier transform and correlation," *Opt. Lett.* **22**, 964–966 (1997).
4. J. Rosen, "Three-dimensional electro-optical correlator," *J. Opt. Soc. Am. A* **15**, 430–436 (1998).
5. J. Rosen, "Three-dimensional joint transform correlator," *Appl. Opt.* **37**, 7538–7544 (1998).
6. Y. Li and J. Rosen, "Three-dimensional pattern recognition with a single two-dimensional synthetic reference function," *Appl. Opt.* **39**, 1251–1259 (2000).
7. Y. Li and J. Rosen, "Three-dimensional correlator with general complex filters," *Appl. Opt.* **39**, 6561–6572 (2000).
8. J. J. Esteve-Taboada, D. Mas, and J. Garcia, "Three-dimensional object recognition by Fourier transform profilometry," *Appl. Opt.* **38**, 4760–4765 (1999).
9. M. Takeda and K. Mutoh, "Fourier transform profilometry for the automatic measurement of 3-D object shapes," *Appl. Opt.* **22**, 3977–3982 (1983).
10. Y. Frauel, E. Tajahuerce, M.-A. Castro, and B. Javidi, "Distortion-tolerant three-dimensional object recognition with digital holography," *Appl. Opt.* **40**, 3887–3893 (2001).
11. O. Matoba, E. Tajahuerce, and B. Javidi, "Real-time three-dimensional object recognition with multiple perspectives imaging," *Appl. Opt.* **40**, 3318–3325 (2001).
12. Y. Li, D. Abookasis, and J. Rosen, "Computer-generated holograms of three-dimensional realistic objects recorded without wave interference," *Appl. Opt.* **40**, 2864–2870 (2001).
13. J. Rosen, "Computer-generated holograms of images reconstructed on curved surfaces," *Appl. Opt.* **38**, 6136–6140 (1999).
14. O. Bryngdahl and F. Wyrowski, "Digital holography—computer-generated holograms," in *Progress in Optics*, E. Wolf, ed. (North-Holland, Amsterdam, 1990), Vol. 28, pp. 1–86.
15. B. V. K. Vijaya-Kumar and L. Hassebrook, "Performance measures for correlation filters," *Appl. Opt.* **29**, 2997–3006 (1990).